Flame Image-Based Burning State Recognition for Sintering Process of Rotary Kiln Using Heterogeneous Features and Fuzzy Integral

Weitao Li, Dianhui Wang, *Senior Member, IEEE*, and Tianyou Chai, *Fellow, IEEE*

***Abstract*—Accurate and robust recognition of burning state for sintering process of rotary kiln plays an important role in the design of image-based intelligent control systems. Existing approaches such as consensus-based methods, temperature-based methods and image segmentation-based methods could not achieve satisfactory performance. This paper presents a flame image-based burning state recognition system using a set of heterogeneous features and fusion techniques. These features, i.e., the color feature, the global and local configuration features, are able to characterize different aspects of flame images, and they can be extracted from pixel values directly without segmentation efforts. In this study, ensemble learner models with four types of base classifiers and five fusion operators are examined with comprehensive comparisons. A total of 482 typical flame images, including 86 over-burning state images, 193 under-burning state images, and 203 normal-burning state images, were used in our experiments. These images were collected from the No. 3 rotary kiln at the Shanxi Aluminum Corporation in China, and labeled by the rotary kiln operational experts. Results demonstrate that our proposed image-based burning state recognition systems outperform other methods in terms of both recognition accuracy and robustness against the disturbance from smoke and dust inside the kiln.**

***Index Terms*—Burning state recognition, heterogeneous features, neural networks (NNs) classifiers, ensemble models, fuzzy integral.**

I. Introduction

COMPUTATIONAL intelligence techniques have received considerable attention from the engineering community due to its cognitive modeling power and learning capability [1]. Over the past years, many successful applications related to complex pattern recognition problems have been reported [2], [3]. Although these intelligent systems have their own characteristics due to the nature of domain applications, they share some common components and properties such as feature extraction, classifier design and decision making. It is desired to extract a set of visual features that can model image contents and distinguish the class from each other accordingly. For classifier design, many learner models, such as neural networks (NNs) [4], support vector machines (SVMs) [5] and extreme learning machines (ELMs) [6], can be employed. Decision making unit helps in assigning class label through fusion operations, such as fuzzy integral [7].

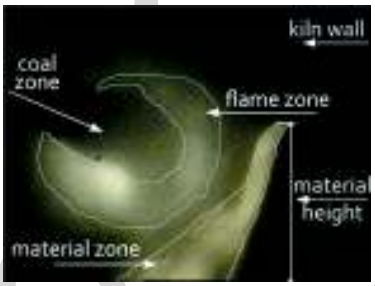

Fig. 1. Burning zone flame image.

It is believed that the burning zone temperature directly reflects the characteristics of the product quality, i.e., clinker. Therefore, an accurate measurement of temperature becomes one of the most critical issues for modeling and controlling the rotary kiln sintering process. Due to the harsh environment inside the kiln, the accurate measurement for such temperature through thermocouple is very challenging. In [8], a single point burning state temperature measurement by a noncontact colorimetric device was employed in developing a rule-based intelligent control system. However, the reporting performance is not favorable and the readings often exhibit big fluctuations due to disturbances from the dust and the smoke inside the kiln.

By observing burning zone flame image (see Fig. 1), including a kiln wall, a coal zone, a material zone, and a flame zone, operators are able to identify the current burning state. This comes from some understandings on the flame images such as: the coal zone is formed by coal powders from the coal burner; the flame zone is formed by instant explosion and combustion of mixed coal powders and air; the material zone is formed by the sintering of raw material slurry. Such a human operating mode is limited by the operator's experience, mental state and working attitude. To overcome these difficulties, flame image analysis-based techniques have been studied over the past years, where a flame image is first segmented into

Manuscript received October 12, 2011; revised January 08, 2012; accepted February 07, 2012. This work was supported in part by the National Basic Research Program of China under Grant 2009CB320601, the Plan for University Subject Innovation and Introducing Intelligence (B08015), and Natural Science Foundation of China under Grant 61020106003, and by a matching grant for 1000 Talent Program (Grant 201100020). Paper no. TII-11-631.

W. Li and T. Chai are with The State Key Laboratory of Synthetical Automation for Process Industries, Northeastern University, Shenyang, Liaoning Province 110004, China (e-mail: lwt1981@yahoo.cn; tychai@mail.neu.edu.cn).

D. Wang is with the Department of Computer Science and Computer Engineering, La Trobe University, Melbourne, VIC 3086, Australia, and also with The State Key Laboratory of Synthetical Automation for Process Industries, Northeastern University, Shenyang, Liaoning Province 110004, China (e-mail: dh.wang@latrobe.edu.au).

Color versions of one or more of the figures in this paper are available online at http://ieeexplore.ieee.org.

Digital Object Identifier 10.1109/TII.2012.2189224

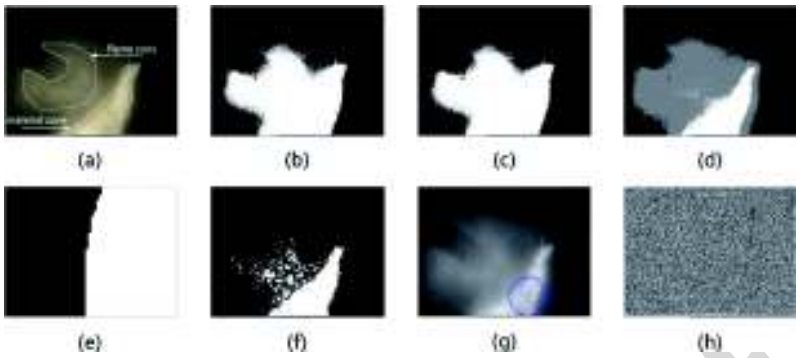

Fig. 2. Performance of image segmentation methods (a) flame image; (b) Ostu [12]; (c) fuzzy c mean and Gabor wavelet (FCMG) [9]; (d) fuzzy c mean (FCM) [13]; (e) normalized cuts [14]; (f) multistage adaptive threshold (MAT) [15]; (g) B-snake [16]; (h) minimax [17].

regions of interest (ROIs), the features of the ROIs are then extracted to recognize the burning states [9] or to identify the concentrations of unburned carbon [11].

From operator's point of view, color, and configurations of the ROIs are two significant features for recognizing the burning states [9]. Previous studies on these feature-based burning state recognition had to apply image segmentation techniques before extracting these features. However, since turbulent flame bounces around, brightness of material zone results from flame zone, and the dust and the smoke couple the ROIs. Hence, allocating the accurate boundary of the ROIs is very challenging. Fig. 2 shows the experimental studies based on several image segmentation methods [9], [12]–[17]. As can be seen that the segmentation will in turn lead to inaccurate feature extraction followed by a poor burning state recognition performance.

To achieve better burning state recognition performance, further efforts on modeling the content of flame images by various features and developing advanced learning classifier systems should be addressed. This paper aims to develop flame image-based burning state recognition systems using heterogeneous features and fuzzy integral. Specifically, we propose a segmentation-free approach for extracting features, where a Gabor filter is employed to distinguish the ROIs from background [18]. Then, the color features are computed by multivariate image analysis (MIA) techniques [19], and the global and local configurations of the ROIs are presented [20], [21]. Also, multiple classifier systems with four types of learner models and five fusion operators are examined. Numerous experimental studies with comprehensive comparisons are carried out. Results indicate that our coalescent feature-based burning state recognition system outperforms the single feature-based methods, image segmentation-based methods and temperature-based methods.

The remainder of the paper is organized as follows. Section II details our approaches for extracting features. Section III describes four types of learner models used in this study, and addresses a fuzzy integral-based fusion method for flame image-based burning state recognition systems. Section IV reports our experimental results with comparisons and discussions. Section V concludes this work and directs further research.

Fig. 3. Fixed windows of flame image.

II. Feature Extraction

A. Preprocessing of Flame Images

It has been reported in [23] that only a subset of a filter bank may be useful, while others are redundant and offer little improvement to (or even reduce) the discriminative power due to the peaking phenomenon [22]. Thus, we propose to incorporate Mahalanobis separability measure and forward selection technique to automatically generate a compact Gabor filter bank, which not only saves computational cost but also aims to enhance the separability of the ROIs.

Because the camera placement provides a rough estimate for the location of the ROIs, two windows with fixed size of 25×25 pixels are used to sample the flame and material zones to avoid the segmentation issue as shown in Fig. 3. Assume a total of $2T_r$ flame and material texture images sampled from T_r gray-scale transformed images of the training RGB flame images $\boldsymbol{I}_1, \boldsymbol{I}_2, \ldots, \boldsymbol{I}_{T_r}$: $\boldsymbol{T}_1, \boldsymbol{T}_2, \ldots, \boldsymbol{T}_{2T_r}$. Let $\boldsymbol{z}_1, \boldsymbol{z}_2, \ldots, \boldsymbol{z}_{n_G}$ denote feature groups extracted by using $n_G = 64$ initial Gabor filters from filtered texture images, where $\boldsymbol{z}_k = [z_{1,k}, z_{2,k}, \ldots, z_{2T_r,k}]^T$, $k = 1, \ldots, n_G$, and parameters of initial Gabor filter bank is set as $f_m = \gamma/(2\gamma + 2\sqrt{\log 2}/\pi)$, $n_f = 4$, $n_o = 4$, $\gamma = 0.5, 1.0$, and $\eta = 0.5, 1.0$ [36]. For each texture image, the mean μ and the standard deviation ϑ features are extracted, i.e., $z_{w,k} = [\mu_{w,k}, \vartheta_{w,k}]$. Mahalanobis separability measure $J_M(k)$ is employed as the metric function to evaluate and sort the discriminative power of $\boldsymbol{z}_k$ and associated filters, i.e.,

$$J_M(k) = (\boldsymbol{m}_{m,k} - \boldsymbol{m}_{n,k})\boldsymbol{C}_k^{-1}(\boldsymbol{m}_{m,k} - \boldsymbol{m}_{n,k})^T \qquad (1)$$

where $\boldsymbol{m}_{m,k}$, $\boldsymbol{m}_{n,k}$, and $\boldsymbol{C}_k$ denote mean vector and covariance matrix of flame class and material class in feature space along feature group $\boldsymbol{z}_k$, respectively.

In this study, a metric is combined with a forward selection technique to automatically select uncorrelated feature groups and associated Gabor filters to best distinguish flame zones and material zones [30].

Once the compact filter bank with n_s Gabor filters for training gray-scale image dataset is selected, they will be applied to the R, G, and B channel subimages of each original flame image respectively. Then, for each training RGB flame image $\boldsymbol{I}$, the mean image $\boldsymbol{I}'$ of n_s filtered images is used as the filtered flame image for further processing.

B. Color Feature

In this work, the MIA techniques proposed in [19] are employed to extract the color feature. The filtered flame images $\boldsymbol{I}'$ are represented by the RGB color model with 8 bits resolution for each channel. MIA technique is based on multiway PCA, which is equivalent to unfold the 3-D image data array $\boldsymbol{I}'$ into an 2-D matrix $\bar{\boldsymbol{I}}'$ without considering the spatial coordinates of pixels, and then performs PCA on it

$$\boldsymbol{I}'_{F_r \times F_c \times 3} \overset{\texttt{unfold}}{\longrightarrow} \bar{\boldsymbol{I}}'_{F \times 3} = \Sigma_{a=1}^{\mathrm{PC}} \boldsymbol{t}_a \boldsymbol{p}_a^T + \bar{\boldsymbol{E}} \tag{2}$$

where $\boldsymbol{I}'$ has the size $F_r \times F_c$, whilst $\bar{\boldsymbol{I}}'$ with the size $F \times 3$, and $F = F_r \times F_c$; $\boldsymbol{t}_a$ are score vectors, and the corresponding $\boldsymbol{p}_a$ are loading vectors.

After scaling and rounding off from 0 to 255, $\boldsymbol{t}_a$ is denoted as $\boldsymbol{s}_a$ and can be refolded into the original image size and displayed as an image. For RGB image, the first two score vectors usually explain 99% of the total variance. Inspection of the $t_1 - t_2$ score plot is a common tool in PCA analysis to detect clusters or outliers. However, due to the numerous number of pixels, many of the pixels may have nearly identical $t_1 - t_2$ values. An analysis from a compressed 256×256 score plot histogram $\mathbf{TT}$ is used to describe the score plot space [24]. $\mathbf{TT}$ can be obtained from scaled and rounded $\boldsymbol{s}_1$ and $\boldsymbol{s}_2$, where each element is computed as

$$TT_{i,j} = \Sigma_b 1, \ (\forall b, s_{1,b} = i, s_{2,b} = j, i, j = 0, \ldots, 255). \tag{3}$$

In such score plot, pixels with similar color in the image space are clustered together in the score space, i.e., each location represents a certain color, and brighter colors indicate histogram bins with higher pixel intensities. Moreover, as the burning states change, the locations of pixels in the score plots change significantly. This enables one to use masking to obtain the ROIs of flame image whose pixels have similar color in the image space to distinguish various burning states.

According to [24], we construct a 256×256 binary masking matrix M, where an element is 1 if its corresponding location of the histogram lies under the masking and 0 if not as shown in Fig. 4. Then, we calculate the area feature A to characterize the color of the training flame image defined as follows:

$$A = \Sigma_{i,j} TT_{i,j} \qquad \forall i, j, M_{i,j} = 1. \tag{4}$$

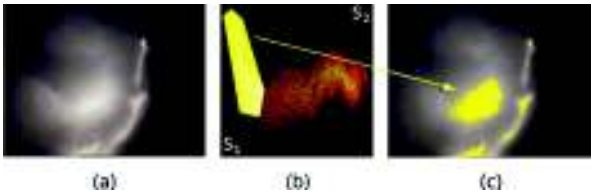

Fig. 4. (a) Original flame image. (b) Score plot of flame image with masking (yellow). (c) Flame image with overlay of highlighted pixels.

C. Global Configuration Feature

Global configuration of the ROIs of flame images, characterizing the heat source, disturbance from the smoke and the dust, and the clinker sintering status, are useful to detect the burning state. Flame zone with good circularity and appropriate material zone height mean proper heat supply, fine ventilation, and satisfied clinker quality which correspond to the normal burning state [9].

Eigen-flame image decomposition based on PCA can be applied to extract global features that represent the global configuration of the flame images. Suppose $\boldsymbol{I}'_1, \boldsymbol{I}'_2, \ldots, \boldsymbol{I}'_{T_r}$ represent T_r filtered training flame images. $\boldsymbol{Y}_1, \boldsymbol{Y}_2, \ldots, \boldsymbol{Y}_{T_r}$ are denoted as these eigen-flame images after applying PCA to the training dataset. Notice that the correlation coefficients between a flame image and the eigen-flame images can be considered as a global feature to represent the flame image, hence the selection for the eigen-flame images is important. Fisher ratio [25] is employed as the metric function to select the eigen-flame images to maximize class separability. The average class separability $J_F(e)$ of the e-th eigen-flame image $\boldsymbol{Y}_e$ can be defined as

$$J_F(e) = \frac{\sum_{i=1}^{N_C} \sum_{j=1}^{N_C} \frac{|g_{i,e} - g_{j,e}|^2}{h_{i,e}^2 + h_{j,e}^2}}{N_C(N_C - 1)} \qquad e = 1, \ldots, T_r \tag{5}$$

where $g_{i,e}$, $g_{j,e}$, $s_{i,e}$, $s_{j,e}$ and N_C denote mean and standard deviation of flame image class C_i, and class C_j correlated with $\boldsymbol{Y}_e$ and the image class number, respectively.

Once the $J_F(e)$ of all $\boldsymbol{Y}_e$ are evaluated, the eigen-flame images selection, i.e., extraction of optimal global features, can be carried out.

D. Local Configuration Feature

Scale invariant feature transform (SIFT) operator is shown to be superior to others in local feature detection and description. Hence, it is employed to extract the local configuration features of the ROIs. Based on image pyramid and gradient histogram, local features extracted by SIFT operator includes keypoint and descriptor. Each SIFT keypoint is denoted as $\boldsymbol{\beta} = \{\boldsymbol{\beta}_i | \boldsymbol{\beta}_i = ((\xi_i, \zeta_i), \delta_i, \theta_i), i \in [1, \tau]\}$, where ξ, ζ, δ, θ, and τ are the coordinates, scale, gradient orientation, and number of the keypoints, respectively. Each 128-dimensional descriptor for each keypoint is created by accumulating the orientation histogram around the keypoint, denoted as $\boldsymbol{\chi} = \{\boldsymbol{\chi}_i | \boldsymbol{\chi}_i = (\chi_{i,1}, \chi_{i,2}, \ldots, \chi_{i,128}), i \in [1, \tau]\}$. Finally, the local configuration will be featured by the combination of SIFT descriptors as shown in Fig. 5, where the direction and length of the arrow denote θ and δ.

To reduce the dimensionality of the local features, a visual vocabulary is constructed via the k-means clustering on the ϖ

Fig. 5. Detected SIFT keypoints of a flame image.

SIFT descriptor vectors from T_r training flame images. Such $N_v (N_v \ll \varpi)$ clustered feature vectors will be considered as "visual words", and then each descriptor of every image is assigned to the nearest cluster to form a co-occurrence table $\bar{\boldsymbol{N}}_{N_v \times T_r}$. The co-occurrence table actually lists the frequency of each visual words in each flame images. Practically, high-dimensional SIFT descriptor is difficult to handle. Exploring research in image and text retrieval, "bag of visual words" (BoVW) [27] and term frequency-inverse document frequency weight [28] are applied to vector quantize the SIFT descriptors into clusters and form the visual word-image table to reduce the dimensionality of local feature representation. For such table, zero-frequency problem [29] might bring sequel, e.g., the classification performance will be affected by synonymy. Latent semantic analysis (LSA) [30] is hence employed to map the original visual word-image space to a latent semantic space by taking advantage of some of the implicit higher-order structure in associations of visual words with images to mitigate such problem and reduce the local feature dimensionality further.

LSA requires the singular value decomposition to generate a semantic space that represents conceptual visual word-image associations, which can be written as

$$\boldsymbol{N}_{N_v \times T_r} = \boldsymbol{U}_{N_v \times N_v} \boldsymbol{\Sigma}_{N_v \times N_v} \boldsymbol{V}^T_{T_r \times N_v} \qquad N_v \ll T_r \tag{6}$$

where $\boldsymbol{U}$, $\boldsymbol{V}$, and $\boldsymbol{\Sigma}$ are the matrices of the visual word vectors, image vectors, and singular values. The best approximation of the visual word-image table $\boldsymbol{N}$ with rank-l is given by selecting the first l values of $\boldsymbol{\Sigma}$ and associated vectors from $\boldsymbol{U}$ and $\boldsymbol{V}$, which can be written as

$$\tilde{\boldsymbol{N}}_l = \tilde{\boldsymbol{U}}_{l \times l} \tilde{\boldsymbol{\Sigma}}_{l \times l} \tilde{\boldsymbol{V}}^T_{T_r \times l} \approx \boldsymbol{U} \boldsymbol{\Sigma} \boldsymbol{V}^T = \boldsymbol{N}. \tag{7}$$

Now, the local configuration can be considered to be conceptually featured by semantic vectors.

It is believed that various semantics offer distinct contributions to burning state recognition. Semantic selection should be carried out by taking their saliency into consideration. For each column of $\boldsymbol{V}$, Mahalanobis measure is used to evaluate and sort the discriminative power of semantic vector $\boldsymbol{v}_r, r = 1, \ldots, N_v$, which is defined as

$$J_M(r) = \frac{\sum_{i=1}^{N_C} \sum_{j=1}^{N_C} (\tilde{\boldsymbol{m}}_{i,r} - \tilde{\boldsymbol{m}}_{j,r}) \tilde{\boldsymbol{C}}^{-1}_{i,j,r} (\tilde{\boldsymbol{m}}_{i,r} - \tilde{\boldsymbol{m}}_{j,r})^T}{N_C (N_C - 1)} \tag{8}$$

where $\tilde{\boldsymbol{m}}_{i,r}$, $\tilde{\boldsymbol{m}}_{j,r}$, and $\tilde{\boldsymbol{C}}_{i,j,r}$ denote mean vector and covariance matrix of flame image class C_i and C_j in semantic space along $\boldsymbol{v}_r$, respectively.

As the classification performance of N_v possible visual word clusters of training flame images tends to be steady, an optimal visual words-images table $\boldsymbol{N}_q$ with q visual words (corresponding an optimal semantic number t), the associated $\tilde{\boldsymbol{V}}_{T_r \times t}$, $\tilde{\boldsymbol{U}}_{t \times t}$ and $\tilde{\boldsymbol{\Sigma}}_{t \times t}$ can be generated from the training dataset. In the same way, the local feature vector of a flame image can be extracted and computed by

$$\tilde{\boldsymbol{d}}^T = \boldsymbol{d}^T \tilde{\boldsymbol{U}}_{t \times t} \tilde{\boldsymbol{\Sigma}}^{-1}_{t \times t}. \tag{9}$$

III. Recognition System Design

With the three kinds of features, burning state recognition systems can be designed using different learner models. To simplify our design, we employ the same type of learner model to build feature classifiers. Then, the fuzzy integral is applied to fuse the base classifiers. Fig. 6 depicts the flowchart of our proposed recognition systems, which are composed of the following components.

- ROIs of input training flame images are distinguished from background based on Gabor filter preprocessing procedure to facilitate the following feature extraction and pattern classification procedure.
- For filtered training flame images, color, global configuration and local configuration features of flame image ROIs are extracted simultaneously.
- Feed each individual feature to the pattern classifier to obtain its burning state recognition result.
- Fuzzy integral fuses the burning state recognition results of three features and gives the final training recognition result.
- Based on the well trained model parameters in the preprocessing, feature extraction, pattern classification, and decision procedure, testing flame images can obtain their final recognition result in the same way.

This section briefly describes the learner models used in our study, and also provides some fundamentals of fuzzy integral.

1) Probabilistic NNs: PNN is constructed based on the well-known Bayesian classification techniques [31]. The extracted feature vectors $\boldsymbol{o}^*$ of testing images are feed into the PNN, and the output of the hidden layer can be computed by

$$\phi_{ij}(\boldsymbol{o}^*) = \frac{1}{(2\pi)^{d_f/2} \sigma^{d_f}} \exp\left[-\frac{\|\boldsymbol{o}^* - \boldsymbol{o}_{ij}\|^2}{2\sigma^2} \right] \tag{10}$$

where $\boldsymbol{o}_{ij}$, d_f, and σ are the jth neuron feature vector of class C_i from the training images, the dimension of $\boldsymbol{o}^*$ and the smoothing parameter, respectively.

The summation layer neurons compute the maximum likelihood of pattern o^* being classified into class C_i by summarizing and averaging the output of all neurons that belong to the same class, i.e.,

$$PB_i(\boldsymbol{o}^*) = \frac{1/N_i}{(2\pi)^{d_f/2} \sigma^{d_f}} \sum_{j=1}^{N_i} \exp\left(-\frac{\|\boldsymbol{o}^* - \boldsymbol{o}_{ij}\|^2}{2\sigma^2} \right) \tag{11}$$

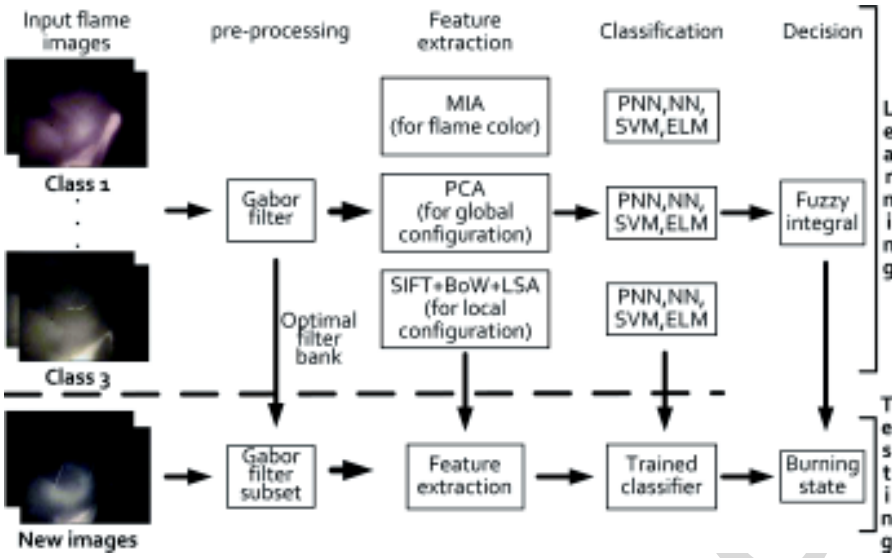

Fig. 6. Flowchart of the burning state recognition systems.

where N_i denotes the total number of training examples from class C_i.

The feature vector $\boldsymbol{o}^*$ is finally classified in accordance with the Bayesian rule based on the outputs of all the summation layer neurons, i.e.,

$$C(\boldsymbol{o}^*) = \arg\max\{PB_i(\boldsymbol{o}^*)\} \qquad i = 1, 2, 3 \tag{12}$$

where $C(\boldsymbol{o}^*)$ denotes the predicted class label of the feature vector o^*.

In PNN, the smoothing parameter σ has a great impact on the recognition performance. According to [37], the σ is computed as

$$\sigma_{\text{opt}} = 1.444 \left[\frac{1}{N_i} \sum_{j=1}^{N_i} \|\boldsymbol{o}_{ij}^* - \boldsymbol{o}_{ij}\|^2 \right]^{1/2} \tag{13}$$

where $\boldsymbol{o}_{ij}^*$ represents the nearest neighbor of $\boldsymbol{o}_{ij}$.

A. Feature Classifiers

1) NNs: Since pattern classification can be considered as a mapping from a feature space to a class label space, we can formalize a NN as a classifier. Assume a single hidden layered NN classifier with d_f, N_{hl}, and N_{ol} neurons in the input, hidden, and output layer, respectively. Let I_w be $N_{hl} \times d_f$ input weights, B_i be $N_{hl} \times 1$ bias of hidden neurons and O_w be $N_C \times N_{hl}$ output weights. The output $\hat{Y} = [\hat{y}_1, \hat{y}_2, \ldots, \hat{y}_{N_C}]$ of the NN is given by

$$\hat{y}_{n_k} = G\left(\sum_{j=1}^{N_{hl}} O_{w_{n_k,j}} G_j(I_w, B_h, \boldsymbol{o}^*) \right) \tag{14}$$

where $G_j(\cdot)$ is the output of the jth hidden neuron and is defined as

$$G_j = G\left(\sum_{n_d=1}^{d_f} I_{w_{jn_d}} \boldsymbol{o}_{n_d}^* + B_{h_j} \right) \tag{15}$$

where $G(\cdot)$ is the activation function, and $j = 1, 2, \ldots, N_{hl}$.

In our case, $N_C = 3$, $N_{hl} = 2 \times d_f + 1$ and the sigmoid function $G(\nu) = 1/(1 + e^{-\nu})$ is used as the activation function of the neurons at the hidden layer and the output layer. Given the training dataset, NN classifiers can be trained by the well-known error back-propagation algorithm.

2) Support Vector Machines: SVM is constructed based on the structural risk minimization principle and mathematical programming techniques. The basic idea of SVM is to map the feature vector $\boldsymbol{o}^*$ from the input space to a transformed space $\varphi(\boldsymbol{o}^*) : \boldsymbol{o}^* \rightarrow \varphi(\boldsymbol{o}^*)$, and then to find a hyper-plane to separate the training data with a minimal misclassification rate, i.e.,

$$\bar{l}(\bar{\boldsymbol{w}} \cdot \varphi(\boldsymbol{o}^*) + \bar{b}) \geq 1 - \epsilon \tag{16}$$

where $\bar{l} \in \{-1, 1\}$, representing class labels. The hyper-plane $\bar{\boldsymbol{w}} \cdot \varphi(\boldsymbol{o}^*) + \bar{b} = 0$ maximizes the margin of separation $2/\|\bar{\boldsymbol{w}}\|$ between two classes. The support vectors can be obtained To maximize the margin and simultaneously minimize the training error, we need to solve an equivalent quadratic programming problem below

$$\begin{aligned} \texttt{Minimize}: & \frac{1}{2}\|\bar{\boldsymbol{w}}^2\| + C_0 \sum_{i=1}^{T_r} \epsilon_i, \\ \texttt{Subject to}: & \bar{l}_i \left(\bar{\boldsymbol{w}} \cdot \varphi(\boldsymbol{o}_i^*) + \bar{b} \right) \geq 1 - \epsilon_i. \end{aligned} \tag{17}$$

A kernel function $K(\cdot, \cdot)$ is usually employed in the implementation of SVM to compute the inner products between the support vectors and the testing feature vectors in the transformed space. The support vectors and parameters used in the decision function can be obtained by solving an equivalent optimization problem as follows:

$$\begin{aligned} \texttt{Minimize}: & \quad \frac{1}{2} \sum_{i=1}^{T_r} \sum_{j=1}^{T_r} \bar{l}_i \bar{l}_j K(\boldsymbol{o}_i^*, \boldsymbol{o}_j^*) \bar{\lambda}_i \bar{\lambda}_j - \sum_{i=1}^{T_r} \bar{\lambda}_i, \\ \texttt{Subject to}: & \quad \sum_{j=1}^{T_r} \bar{l}_i \bar{\lambda}_i = 0, \quad 0 \leq \bar{\lambda}_i \leq C_0, \end{aligned} \tag{18}$$

where each Lagrange multiplier $\bar{\lambda}_i$ corresponds to a training example $\boldsymbol{o}_i^*$. In our study, the Gaussian kernel function

$K(u,v) = \exp(-\delta\|u-v\|^2)$ is applied. Moreover, cost parameter C and kernel parameter δ are selected as $C_0 \in \{2^{12}, 2^{11}, \ldots, 2^{-1}, 2^{-2}\}$ and $\delta \in \{2^4, 2^3, \ldots, 2^{-9}, 2^{-10}\}$.

3) Extreme Learning Machines: ELM is a class of random base function approximators which are represented as single layer feed-forward NNs (readers can find more details in [6]). In ELM, the input weights I_w and hidden biases B_h are randomly generated. The hidden layer maps the inputs $\boldsymbol{o}_i^*$ into a feature space via a nonlinear transformation $H = G(I_w \cdot \boldsymbol{o}_i^* + B_h)$, whilst the output layer performs like a linear combiner. Given a hidden node number N_{hl}, the output weights can be computed as

$$O_w = H^{\dagger}Y \tag{19}$$

where $Y = [Y_1, Y_2, \ldots, Y_{T_r}]^T$ is the expected output matrix, $H^{\dagger} = (H^T H)^{-1} H^T$ is a Moore–Penrose generalized inverse of the hidden layer output matrix H.

Compared against traditional gradient-based learning algorithms, ELM is extremely fast whilst better generalization performance can be obtained if an appropriate number of hidden neurons is chosen. In this study, the sigmoid function $G(\nu) = 1/(1+e^{-\nu})$ is used as the activation function and the number of hidden neurons N_{hl} is set as seventy.

B. Fusion of Feature-Based Burning State Classifiers

The fuzzy integral is a nonlinear function that is defined based on a fuzzy measure, especially g_λ-fuzzy measure, which provides an effective way to fuse information. For classification problem, the fuzzy integral combines the outputs of base classifiers with importance of each classifier, which is subjectively assigned as the nature of fuzzy logic. The following gives some basics of the fuzzy integral used in this study.

Definition 1: Let X be a finite set of elements. Let $g: 2^X \to [0,1]$ with satisfying the following conditions:

1) $g(\leq) = 0$;
2) $g(X) = 1$;
3) $g(O) \leq g(P)$ if $O \subset P$;
4) $g(O \cup P) = g(O) + g(P) + \lambda g(O)g(P), (\lambda > -1)$, if $O, P \subset X$ and $O \cap P = \leq$.

Then, g is called a g_λ-fuzzy measure.

Definition 2: Let X be a finite set, and $h: X \to [0,1]$ be a fuzzy subset of X. The fuzzy integral over X of the function h, with respect to a fuzzy measure g is defined as

$$\begin{aligned} h(x) \circ g(\cdot) &= \max_{E \subseteq X}[\min(\min_{x \subseteq E} h(x), g(E))] \\ &= \max_{\bar{\alpha} \in [0,1]}[\min(\alpha, g(h_o))] \end{aligned} \tag{20}$$

where h_o is the $\bar{\alpha}$ level set of h

$$h_o = \{x | h(x) \geq \bar{\alpha}\}. \tag{21}$$

The fuzzy integral has the following properties.

1) If $h(x) = c$, for all $x \in X$, $0 \leq c \leq 1$, then

$$h(x) \circ g(\cdot) = c.$$

2) If $h_1(x) \leq h_2(x)$ for all $x \in X$, then

$$h_1(x) \circ g(\cdot) \leq h_2(x) \circ g(\cdot).$$

3) If $B_i | i = 1, \ldots, \iota$ is a partition of the set X, then

$$h(x) \circ g(\cdot) \geq \max_{i=1}^{\iota} \varepsilon_i,$$

where ε_i is the fuzzy integral of h with respect to g over B_i.

The calculation of the fuzzy integral is as follows: let $X = \{x_1, x_2, \ldots, x_\iota\}$ and $f = \{f_1, f_2, \ldots, f_{N_c}\}$ be a set of classifiers and classes of the flame images for one time burning state recognition respectively, and let $h_\varrho : X \longrightarrow [0,1]$ be the evaluation of how certain a flame image $\boldsymbol{I}$ belongs to the class f_ϱ using the classifier x_i, where 1 indicates absolute certainty and 0 implies absolute uncertainty. The fuzzy integral ε over X with respect to a fuzzy measure g can be defined by

$$\varepsilon = h(x) \circ g(\cdot) = \max_{i=1}^{\iota}[\min(h(x_i), g(B_i))] \tag{22}$$

where $B_i = \{x_1, x_2, \ldots, x_i\}$, g is a g_λ-fuzzy measure, and $g(B_i)$ can be computed recursively as follows:

$$g(B_1) = g(x_1) = g^1, \tag{23}$$

$$g(B_i) = g^i + g(B_{i-1}) + \lambda g^i g(B_{i-1}) (1 < i \leq \iota) \tag{24}$$

where λ is solution of the following equation:

$$\lambda + 1 = \prod_{i=1}^{\iota}(1 + \lambda g^i) \tag{25}$$

where $\lambda \in (-1, +\infty)$ and $\lambda \neq 0$.

To compute the fuzzy integral, we need to know the density function g^i for each x_i, which illustrates the importance of various classifiers for the final burning state recognition. These densities can be assigned by experts via trial-and-error or produced from training dataset. In our study, the soundness of each classifier is defined by the classification accuracy over the training dataset, and is used to describe the g_ϱ^i. The classification rates of the same classifier over the test dataset are used to describe the h_ϱ^i.

IV. Experimental Results

In order to validate the presented method, flame images of the burning zone under various conditions are collected from No. 3 rotary kiln at Shanxi Aluminum Corporation. A color CCD camera (Panasonic WV-CP450) and a noncontact colorimetric temperature measure device are installed outside the peephole of the kiln head. The output signal of CCD is digitized using an image grabber card (Matrox Meteor II). Each digital image has a size of 512×384 pixels, and each pixel is composed of red (R), green (G), and blue (B) components. The sampling period for flame image and burning zone temperature is set to 10 s.

According to three rotary kiln operators' judgement, the collected flame images were labelled by voting method as over-burning, under-burning, and normal-burning classes respectively. Some minor adjustment on the labels class were done by operational experts from Shanxi Aluminum Corporation to justify our results reported in this paper. A total of 482 typical flame images, including 86 over-burning state images, 193 under-burning state images, and 203 normal-burning state images are selected from 4150 flame images to form the sample dataset. Based on bootstrapping [32] with 2000 replica, training and testing dataset are performed to estimate the accuracy of

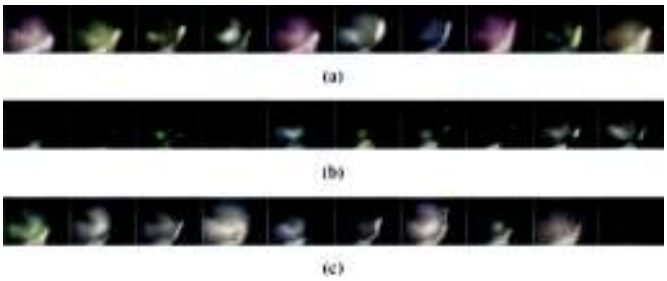

Fig. 7. (a) Over-burning. (b) Under-burning. (c) Normal-burning.

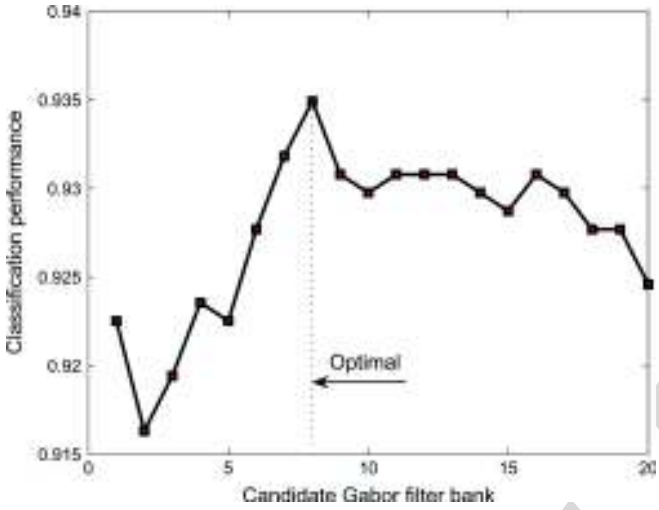

Fig. 8. Classification result versus candidate Gabor filter bank.

the flame image burning state recognition. Some flame image examples are shown in Fig. 7.

A. Experiments for Gabor Filter Preprocessing

Fig. 8 shows the classification result of the training flame and material texture images with respect to the candidate Gabor filter bank used during one sampling experiment. As shown in Fig. 8, the optimal recognition result is achieved when the eight most discriminative Gabor filters are used. Thus, such a compact filter bank is selected to filter the training and testing flame images throughout this sampling experiment.

It is worth noting that a peaking phenomenon occurs in the Gabor filter bank design procedure, i.e., the high-dimensional feature representation leads to a gradual degradation classification performance. Hence, in design of Gabor filter bank, from our understandings, it should not be a simple procedure of subjectively seeking filter parameters and creating filter bank, selection of filter candidates is an indispensable part for such a procedure to avoid the possible peaking phenomenon.

The effectiveness of our Gabor filter bank designing method for discriminating ROIs is tested compared with other designing methods with 2000 repeats listed in Table I. From Table I, as we can see, our filter bank design approach not only selects the uncorrelated filters and leads to a more compact filter bank, but also distinguishes the flame and material zones much more to facilitate the sequel.

TABLE I
COMPARISON RESULTS FOR VARIOUS GABOR FILTER DESIGNING METHODS

Gabor filter design methods	Average accuracy (%)	No. of Gabor filters
Presented method	93.69±1.4	5.8±1.9
Fisher ratio-based	93.21±1.5	6.4±3.0
D.A. Clausi-based [33]	90.41±1.9	24
S. Li-based [34]	89.30±2.1	36
F. Bianconi-based [35]	90.65±1.9	288

TABLE II
COMPARISON RESULTS FOR THE FLAME COLOR-BASED METHODS

	Presented method	Global color-based
PNN	81.25±4.7	76.26±5.4
NN	75.13±2.0	72.24±2.3
SVM	85.55±1.5	81.54±1.5
ELM	77.00±1.2	72.35±1.0

B. Experiments Based on Flame Color

Following the steps presented in Section II, MIA is firstly performed on each training flame image, and then in the compressed score space, the area feature A is computed to characterize the flame color through masking procedure. In the present study, four classifiers, i.e., PNN, NN, SVM, and ELM, are applied to perform pattern classification for the burning state recognition subresult respectively as listed in Table II with mean values ± standard deviations of 2000 repeats. To avoid the difficult segmentation of ROIs, we have also tested the performance of the global color-based method.

In Table II, as we can see, the disturbance of smoke and dust has great effect on the performance of the flame color-based method. However, as a primary recognition for burning state, the result can be accepted. Moreover, MIA can eliminate much of the unstructured noise and extract more meaningful ROIs from the original flame image. In contrast, the global color-based method contains some disturbances and redundant information. The result is hence inferior to the presented flame color-based method. Further, various classifiers offer discriminative power for pattern classification. At such feature, SVM outperforms the other three classifiers.

C. Experiments Based on Global Feature of Flame Image

Fig. 9 shows the burning state recognition accuracy corresponding to the candidate eigen-flame image combinations used, i.e., the number of global features. In Fig. 9, peaking phenomenon also occurs and 100% accuracy is achieved on the training dataset when the six most discriminative eigen-flame images are used. Thus, such six eigen-flame images are selected for the testing flame images throughout this sampling experiment.

The significant degree of our eigen-flame image selection algorithm for global feature extraction is tested compared with traditional eigen-flame image selection method with 2000 repeats listed in Table III, respectively. Moreover, the impact of various classifiers for the global feature of flame image are also studied as shown in Table IV.

From Tables III–IV, we have the following observations.

1) Independently of eigen-flame image selection method, our Gabor filter preprocessing approach discriminates the

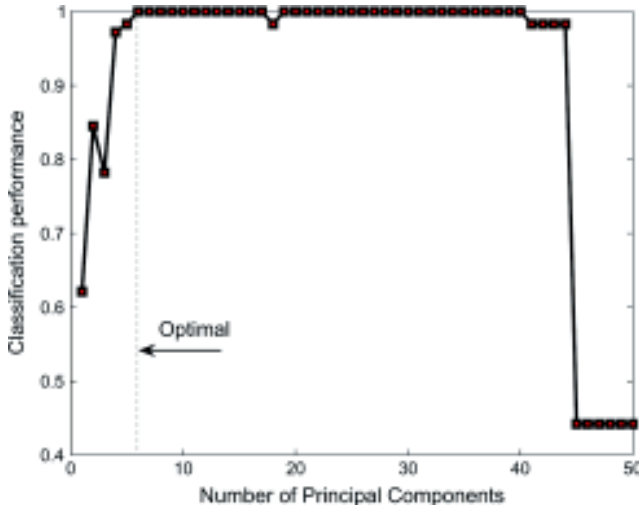

Fig. 9. Classification result versus Number of eigen-flame images.

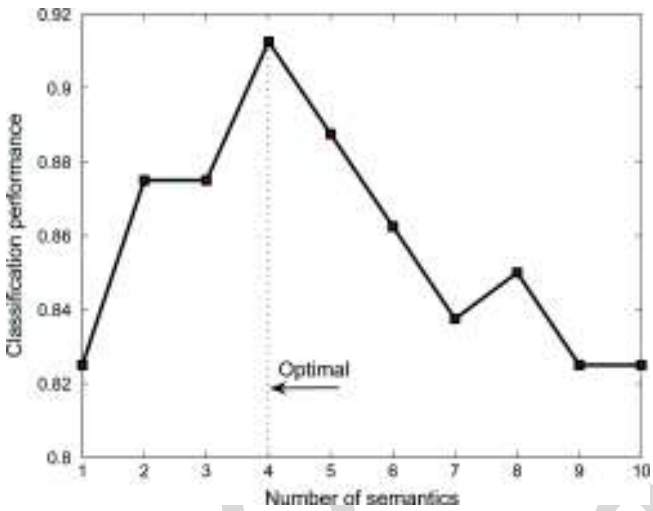

Fig. 10. Classification result versus candidate semantic vector subsets.

TABLE III
COMPARISON RESULTS FOR THE GLOBAL FEATURE-BASED METHODS

	With eigen images selection	Without eigen images selection
Accuracy (with filter)	88.57±2.7	83.88±2.8
Accuracy (without filter)	83.44±3.1	78.21±3.4
No. of PC (with filter)	6.9±2.3	7.5±2.1
No. of PC (without filter)	7.4±2.2	8.2±2.2

TABLE IV
COMPARISON RESULTS FOR VARIOUS CLASSIFIERS (GLOBAL FEATURE)

	Average accuracy (%)	No. of PC
PNN	88.57±2.7	6.9±2.3
NN	87.72±2.5	9.5±2.1
SVM	86.42±2.1	5.6±1.5
ELM	88.53±2.0	9.3±2.0

ROIs much more to facilitate the sequel. Moreover, the global feature is not only more robust than the flame color, but also avoids the difficult segmentation of the ROIs.

2) By selecting the eigen-flame images, the global feature obtained substantially outperform those without selection. This is because PCA is optimal from a low-dimensional reconstruction viewpoint and is nonoptimal from the pattern classification point of view.
3) PNN is essentially based on the well-known Bayesian classification technique, and considers the probability characteristic of sample space. Therefore, although the number of principal components is not minimum, the classification performance has the best result.

D. Experiments Based on Local Feature of Flame Image

For our flame images, the number of SIFT keypoints is typically 16. Thus, in our study, the maximum dictionary size N_v is set as fifteen and the number of semantics N_{sem} in the sense of N_v visual words is defined as

$$N_{\text{sem}} = \begin{cases} N_v - 1 & 2 \le N_v \le 10 \\ 10 & 10 \le N_v \le 15. \end{cases} \tag{26}$$

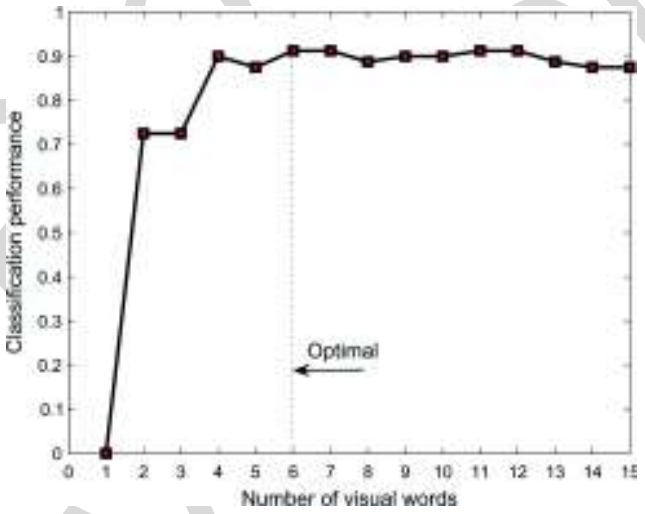

Fig. 11. Classification result versus number of visual words.

Based on the procedure proposed in Section II, Fig. 10 gives the classification result of the training image dataset with respect to the candidate semantic subsets with fifteen visual words during one sampling experiment. In Fig. 10, optimal result is obtained when the four most discriminative semantics are used. Such a semantic subset is selected in the sense of fifteen visual words for the testing image burning state recognition. Please note, in LSA, peaking phenomenon also appears, i.e., excessive insignificant semantics leading to the over-fitting problem. Therefore, LSA should not be a simple procedure of creating the semantic vectors and semantic selection should be an indispensible part in order to take into account their saliency for the burning state recognition.

Fig. 11 shows the burning state recognition accuracy corresponding to the number of visual words, where each point is obtained based on the classification result of the optimal semantic subset under corresponding visual word number. In Fig. 11, the highest recognition rate is achieved on the training dataset with seven visual words. Such seven visual words are selected to construct the dictionary for testing images throughout this sampling experiment.

TABLE V
COMPARISON RESULTS FOR THE LOCAL FEATURE-BASED METHODS

Various methods	Average accuracy(%)	No. of visual words	No. of semantics
Presented method	92.12±1.3	6.2±1.7	4.0±1.1
Standard LSA-based	89.21±1.2	7	4
Stop list-based [27]	87.46±1.4	7	-
Tf-idf table-based	85.62±1.8	7	-
Method (without filter)	90.24±1.7	7.4±1.9	5.1±1.8

TABLE VI
COMPARISON RESULTS FOR VARIOUS CLASSIFIERS (LOCAL FEATURE)

	Average accuracy (%)	No. of visual words	No. of semantics
PNN	92.12±1.3	6.2±1.7	4.0±1.1
NN	83.04±2.4	8.5±1.3	7.9±1.3
SVM	88.12±2.8	9.2±1.3	8.2±1.0
ELM	89.54±1.6	9.1±1.4	8.2±1.2

Taking PNN classifier for instance, the classification accuracy of 2000 repeats is listed in Table V. In order to validate the effectiveness of our semantic selection method for the burning state recognition, we have tested the performance of standard LSA with the same number of visual words and semantic vectors. Further, based on the stop list analogy [27], we select the frequent visual words that occur in all flame images for the burning state recognition. Finally, the performance of the standard tf-idf indexing table-based method is also included in Table V.

From Table V, we have the following observations.

1) Our Gabor filter bank preprocessing approach also facilitates the local feature extraction. Moreover, our method is feasible to extract local feature directly from the flame image for the burning state recognition to avoid the segmentation issue, and can select more salient and discriminative semantics than the standard LSA-based method to form the more meaningful local feature, and hence outperforms it with the same visual word number and semantic vector number.
2) LSA can extract more meaningful semantics than the visual words, which not only generates low-dimensional feature representation to mitigate the problem of synonymy, but also improves the classification performance.
3) During the stop list analogy, frequency is used to represent the significance for the visual words in a certain degree. The removal of the most frequent and infrequent visual words can remove the common and rare words to improve the classification performance. However, evaluation of the discriminative power of the visual words is not involved in such method, and the performance is hence interior.

Further, the discriminative power offered by various classifiers for the burning state recognition is also studied. The performance of our burning state recognition algorithm combined with various classifiers are shown in Table VI. Also, in this local feature-based method, PNN not only outperforms the best result, but also generates the minimum number of visual words and semantic vectors than the NN, SVM, and ELM classifiers.

TABLE VII
FUZZY DENSITIES AND CORRESPONDING λ

Subject	g^1	g^2	g^3	λ
Over-burning	0.9076	0.5630	0.8824	-0.9988
Under-burning	0.9444	0.7821	0.9701	-0.9996
Normal-burning	0.8472	0.8210	0.9563	-0.9948

TABLE VIII
EXAMPLE OF CLASSIFIER OUTPUTS

Subject	$h(x_i)$	$g(B_i)$	$H(E)$	$max[H(E)]$
Over-burning	0.1539	$g(\{x_2\}) = 0.5630$	0.1539	
	0.0305	$g(\{x_2, x_3\}) = 0.9512$	0.0305	0.1539
	0.0201	$g(\{x_1, x_2, x_3\}) = 1$	0.0201	
Under-burning	0.8595	$g(\{x_2\}) = 0.7821$	0.7821	
	0.1005	$g(\{x_2, x_1\}) = 0.9882$	0.1005	0.7821
	0.0712	$g(\{x_1, x_2, x_3\}) = 1$	0.0712	
Normal-burning	0.9970	$g(\{x_3\}) = 0.9563$	0.9563	
	0.9947	$g(\{x_3, x_1\}) = 0.9943$	0.9943	0.9943
	0.4875	$g(\{x_1, x_2, x_3\}) = 1$	0.4875	

E. Recognition Performance Based on Integrated Results

After acquiring the above-mentioned results based on individual features, the final recognition result can be achieved by using the fuzzy integral fusion operation. Firstly, for the training dataset, a set of fuzzy densities g_ϱ^i are given by recognition accuracy of each subrecognition method for each flame image class. Then, the unique root λ greater than -1 for (25) can be computed. Table VII shows the computation results in one sampling experiment with PNN classifier. Suppose that the probabilities of the PNN classifiers' output classes for a testing normal-burning flame image are shown as following, $h(x_1) = 0.0201$, $h(x_2) = 0.1539$, and $h(x_3) = 0.0305$, for over-burning class; $h(x_1) = 0.1005$, $h(x_2) = 0.8595$, and $h(x_3) = 0.0712$, for under-burning class; $h(x_1) = 0.9947$, $h(x_2) = 0.4875$, and $h(x_3) = 0.9970$, for normal-burning class, where x_1, x_2, and x_3 are the PNN classifiers with the flame color feature, the global configuration feature, and the local configuration feature, respectively. Table VIII shows how the procedure of the fuzzy integral is formed, where $H(E) = \min(h(x_i), g(B_i))$. Finally, the normal-burning class is assigned as the output of the testing image.

With the same procedure, the average classification accuracy over 2000 runs using various fusion operators and classifiers is shown in Table IX, where same classifier is assigned to three recognition methods during integration, and the recognition probability h of various classifiers for flame image classes and recognition methods is set as the output value for the NN classifiers, one or zero for the SVM classifiers, and output value for the ELM classifiers, respectively. Moreover, we concatenate the above-mentioned individual features extracted, and then recognize the burning state with various pattern classifiers. Our obtained results are reported in Table IX. As can be seen that the recognition performance with the fuzzy integral consensus method outperforms base classifiers, other multiple classifiers with other fusion operators, and the concatenate feature-based classifiers. The results show that good classification performance comes from the objective evidence provided by various classifiers and the subjective expectation of the importance of that evidence. Also, it has been noticed that the PNN, NN, and SVM classifiers with the concatenate feature does not improve

TABLE IX
COMPARISON RESULTS FOR VARIOUS FUSION OPERATORS AND CLASSIFIERS

Methods	PNN	NN	SVM	ELM
Majority	83.14±2.7	79.75±2.6	89.25±1.7	89.83±2.1
Borda count	81.58±2.1	78.45±3.7	87.79±1.5	88.23±3.1
Average	80.24±2.4	76.82±4.2	87.15±1.5	88.32±3.2
Concatenate	90.49±3.3	88.92±4.0	90.12±4.3	92.75±2.8
Fuzzy integral	95.37±2.3	88.41±3.7	91.41±2.8	91.46±3.2

TABLE X
BURNING STATE RECOGNITION RESULTS FOR DIFFERENT IMAGE SEGMENTATION-BASED METHODS

Methods	PNN	NN	SVM	ELM
Ostu	42.67±11.4	40.26±11.1	41.79±11.2	42.13±11.2
FCMG	44.72±12.3	41.62±12.5	42.83±12.1	46.45±9.1
DFM	47.23±11.5	44.31±12.3	46.32±13.2	49.63±10.1
MAT	52.19±11.3	49.29±12.3	51.78±11.3	55.79±9.2

the final result, and the obtained results are even inferior to the results obtained by individual feature-based classifiers.

F. Contrasted Experiments

This section compares our flame image-based method with other existing burning state recognition methods. Firstly, we compared our method with the temperature-based burning state recognition method. Taking the labeling by kiln operational experts as ground truth, the recognition accuracy of the two methods is 95.37% and 81.34% at the same time. Again, our flame image-based method outperforms the temperature-based method and is more reliable even with the disturbance of dust and smoke inside the kiln.

Then, we compared such flame image-based method with four feasible image segmentation-based methods, including Ostu [12], fuzzy c-mean and Gabor wavelet (FCMG) [9], dual fast marching (DFM) [10], and multistage adaptive threshold (MAT) [36]. Also, all experimental studies are in HSV color space. Based on the experience of kiln operational experts, the following sixteen features are extracted to characterize the flame color and the configuration of ROIs, namely average brightness of V subimage, average brightness and its variance of the flame and material zones of V subimage, area, length, width, circularity, and barycentric coordinates of the flame zone, and height, width, area, and barycentric coordinates of the material zone. All these features are then sent to the PNN pattern classifier to obtain the recognition result. The average classification accuracy of 2000 repeats with different classifiers is shown in Table X. In our study, ELM gives the best recognition result except Ostu-based method. This is probably because Ostu is a general-purpose image segmentation method whilst the other methods are special methods for flame image or better image segmentation method. Moreover, obviously, although image segmentation based feature extraction has been successfully applied to many image recognition applications, in our application, the flame images are of poor quality due to the smoke and dust inside the kiln, and this in turn results in inaccurate ROIs segmentation and feature extraction. The above image segmentation-based methods are substantially inferior to any individual of the presented methods and the integrated method that are without the image segmentation procedure, and could work well only when the flame image is of high quality.

V. CONCLUSION

In this study, we have explored the feasibility of applying multifeature integration method to recognize the flame image burning state for the rotary kiln without the difficult segmentation procedures. Firstly, an improved compact Gabor filter bank as the preprocessing step is used to discriminate the ROIs with distinct texture characteristics to facilitate the subsequent feature extraction and burning state recognition. Then, MIA is employed to extract feature to characterize the flame image color. Again, an improved eigen-flame image decomposition technique is used to extract the global configuration features of flame images. Finally, SIFT operator combined with the BoVW image descriptor and an improved LSA is applied to extract the local configuration features. The final recognition result is based on the integration of the classification results of above heterogeneous features by fuzzy integral. Comprehensive experiments were carried out, where the concatenate feature-based method, temperature-based method, and image segmentation-based methods were compared against our proposed systems with various fusion operations. Experimental results have demonstrated the feasibility and effectiveness of our proposed approach.

Our further work is to incorporate the proposed flame image-based burning state recognition system into our previously developed hybrid control system for rotary kiln. It is being expected that an improved product quality index could be achieved by using this image-based sensor.

REFERENCES

[1] A. Kusiak and F. Salustri, "Computational intelligence in product design engineering: Review and trends," *IEEE Trans. Syst., Man, Cybern.—Part C: Appl. Rev.*, vol. 37, no. 5, pp. 766–778, Sep. 2007.
[2] G. Acciani, G. Brunetti, and G. Fornarelli, "Application of neural networks in optical inspection and classification of solder joints in surface mount technology," *IEEE Trans. Ind. Inform.*, vol. 2, no. 3, pp. 200–209, Aug. 2006.
[3] A. Picon, O. Ghita, P. F. Whelan, and P. M. Iriondo, "Fuzzy spectral and spatial feature integration for classification of nonferrous materials in hyperspectral data," *IEEE Trans. Ind. Informat.*, vol. 5, no. 4, pp. 483–494, Nov. 2009.
[4] S. B. Park, J. W. Lee, and S. K. Kim, "Content-based image classification using a neural netwrk," *Pattern Recognit. Lett.*, vol. 25, no. 3, p. 287C300, 2004.
[5] V. N. Vapnik, *The Statistical Learning Theory*. New York: Wiley, 1998.
[6] G. B. Huang, D. H. Wang, and Y. Lan, "Extreme learning machines: A survey," *Int. J. Mach. Learning Cybern.*, vol. 2, pp. 107–122, 2011.
[7] M. Sugeno, "Fuzzy measures and fuzzy integrals: A survey," in *Fuzzy Automata and Decision Processes*. Amsterdam: The Netherlands, 1977.
[8] X. J. Zhou and T. Y. Chai, "Pattern-based hybrid intelligent control for rotary kiln process," in *IEEE Int. Conf. Control Appl.*, Oct. 2007, pp. 31–35.
[9] P. Sun, T. Y. Chai, and X. J. Zhou, "Rotary kiln flame image segmentation based on FCM and Gabor wavelet based texture coarseness," in *Proc. 7th World Congr. Intell. Control Automat.*, Jul. 2008, pp. 7615–7620.
[10] H. Y. Jiang, X. L. Cui, X. J. Zhou, and T. Y. Chai, "Image segmentation based on improved dual fast marching method," *J. Syst. Simul.*, vol. 3, no. 20, pp. 803–810, Feb. 2008.
[11] M. Shimoda, A. Sugano, T. Kimura, Y. Watanabe, and K. Ishiyama, "Prediction methods of unburnt carbon for coal fired utility boiler using image processing technique of combustion flame," *IEEE Trans. Energy Conv.*, vol. 5, no. 4, pp. 640–645, Dec. 1990.
[12] N. Otsu, "A threshold selection method from gray-level histogram," *IEEE Trans. Syst., Man, Cybern.*, vol. SMC–9, no. 1, pp. 62–66, Jan. 1979.

[13] J. C. Dunn, "A fuzzy relative of the ISODATA process and its use in detecting compact well-separated clusters," *J. Cybern.*, vol. 3, no. 3, pp. 32–57, 1973.
[14] J. B. Shi and J. Malik, "Normalized cuts and image segmentation," *IEEE Trans. Pattern Anal. Mach. Intell.*, vol. 22, no. 8, pp. 888–905, Aug. 2000.
[15] F. X. Yan, H. Zhang, and C. R. Kube, "A multistage adaptive thresholding method," *Pattern Recognit. Lett.*, vol. 26, no. 8, pp. 1183–1191, Jun. 2005.
[16] G. Dong, N. Ray, and S. T. Acton, "Intravital leukocyte detection using the gradient inverse coefficient of variation," *IEEE Trans. Med. Imag.*, vol. 24, no. 7, pp. 910–924, Jul. 2005.
[17] B. N. Saha and N. Ray, "Image thresholding by variational minimax optimization," *Pattern Recognit.*, vol. 42, no. 5, pp. 843–856, May 2009.
[18] M. Idrissa and M. Acheroy, "Texture classification using Gabor filters," *Pattern Recognit. Lett.*, vol. 23, no. 9, pp. 1095–1102, Jul. 2002.
[19] P. Geladi and H. Grahn, *MultiVariate Image Analysis*. New York: Wiley, 1996.
[20] J. Yang, D. Zhang, A. F. Frangi, and J. Y. Yang, "Two-dimensional PCA: A new approach to appearance-based face representation and recognition," *IEEE Trans. Pattern Anal. Mach. Intell.*, vol. 26, no. 1, pp. 131–137, Jan. 2004.
[21] D. G. Lowe, "Distinctive image features from scale-invariant keypoints," *Int. J. Comput. Vis.*, vol. 60, no. 2, pp. 91–110, Nov. 2004.
[22] A. K. Jain, R. P. W. Duin, and J. C. Mao, "Statistical pattern recognition: A review," *IEEE Trans. Pattern Anal. Mach. Intell.*, vol. 22, no. 1, pp. 4–37, Jan. 2000.
[23] W. T. Li, K. Z. Mao, H. Zhang, and T. Y. Chai, "Designing compact Gabor filter banks for efficient texture feature extraction," in *Proc. Int. Conf. Control, Automat., Robot. Vis.*, 2010, pp. 1193–1198.
[24] H. L. Yu and J. F. MacGregor, "Monitoring flames in an industrial boiler using multivariate image analysis," *AIChE J.*, vol. 50, no. 7, pp. 1474–1483, Jul. 2004.
[25] R. O. Duda and P. E. Hart, *Pattern Classification and Scene Analysis*. New York: Wiley, 1973.
[26] W. T. Li, K. Z. Mao, X. J. Zhou, T. Y. Chai, and H. Zhang, "Eigenflame image-based robust recognition of burning states for sintering process control of rotary kiln," in *IEEE Conf. Decision Control*, Dec. 2009, pp. 398–403.
[27] J. Sivic and A. Zisserman, "A video Google: A text retrieval approach to object matching in videos," in *Proc. 9th IEEE Int. Conf. Comput. Vis.*, Oct. 2003, pp. 1470–1477.
[28] R. B. Yates and B. R. Neto, *Modern Information Retrieval*. New York: ACM Press, 1999.
[29] I. H. Witten and T. C. Bell, "The zero-frequency problem: Estimating the probabilities of novel events in adaptive text compression," *IEEE Trans. Inf. Theory*, vol. 37, no. 4, pp. 1085–1094, Jul. 1991.
[30] S. C. Deerwester, S. T. Dumais, T. K. Landauer, G. W. Furnas, and R. A. Harshman, "Indexing by latent semantic analysis," *J. Amer. Soc. Inf. Sci.*, vol. 41, no. 6, pp. 391–407, 1990.
[31] D. F. Specht, "Probabilistic neural network," *Neural Network*, vol. 3, no. 1, pp. 109–118, 1990.
[32] M. R. Chemick, *Bootstrap Methods: A Practitioner's Guide*. New York: Wiley, 1999.
[33] D. A. Clausi and H. Deng, "Design-based texture feature fusion using Gabor filters and co-occurrence probabilities," *IEEE Trans. Image Process*, vol. 14, no. 7, pp. 925–936, Jul. 2005.
[34] S. Li and J. S. Taylor, "Comparison and fusion of multiresolution features for texture classification," *Pattern Recognit. Lett.*, vol. 26, no. 5, pp. 633–638, Apr. 2004.
[35] F. Bianconi and A. Fernández, "Evaluation of the effects of Gabor filter parameters on texture classification," *Pattern Recognit.*, vol. 40, no. 12, pp. 3325–3335, Dec. 2007.
[36] F. X. Yan, H. Zhang, and C. R. Kube, "A multistage adaptive thresholding method," *Pattern Recognit. Lett.*, vol. 26, no. 8, pp. 1183–1191, Jun. 2005.
[37] R. E. Shaffer, S. L. Rose-Pehrsson, and R. A. McGill, "A comparison study of chemical sensor array pattern recognition algorithms," *Analytica Chimica Acta*, vol. 384, no. 1, pp. 305–317, Apr. 1999.
[38] T. Hastie, R. Tibshirani, and J. Friedman, *The Elements of Statistical Learning: Data Mining, Inference and Prediction*. NewYork: Springer-Verlag, 2001.

Weitao Li received the B.Sc. and M.Sc. degrees from the Hefei University of Technology, Hefei, China, in 2004 and 2007, respectively. He is currently working toward the Ph.D. degree at Northeastern University, Shenyang, China.

His research interests include image processing and pattern recognition.

Dianhui Wang (SM'03) received the Ph.D. degree from Northeastern University, Shenyang, China, in 1995.

From 1995 to 2001, he worked as a Postdoctoral Fellow with Nanyang Technological University, Singapore, and a Researcher with The Hong Kong Polytechnic University, Hong Kong, China. He is currently a Reader and Associate Professor with the Department of Computer Science and Computer Engineering, La Trobe University, Melbourne, Victoria, Australia. He is also associated with The State Key Laboratory of Synthetical Automation of Process Industries, Northeastern University. His current research interests include data mining and computational intelligence systems for bioinformatics and engineering applications.

Tianyou Chai (M'90–SM'97–F'08) received the Ph.D. degree in control theory and engineering from Northeastern University, Shenyang, China, in 1985.

He is the Director of The State Key Laboratory of Synthetical Automation of Process Industries, Northeastern University. His current research interests include adaptive control, intelligent decoupling control, and integrated automation of industrial process.

Dr. Chai was elected as a member of the Chinese Academy of Engineering in 2003, an Academician of the International Eurasian Academy of Sciences in 2007, and an International Federation of Automatic Control Fellow in 2008.